Robust Control Invariant Sets and Lyapunov-Based MPC for IPM Synchronous Motor Drives

Matthias Preindl, *Member, IEEE*

***Abstract*—This paper proposes a novel simplified model predictive control (MPC) scheme for interior permanent-magnet synchronous machines (PMSM) drive systems. The control problem is formulated in the $\alpha\beta$ stator flux space. The current–flux relation is eliminated from the MPC formulation and can be implemented as nonlinear map or an affine approximation without affecting the MPC complexity. The model is combined with the Lyapunov-based MPC concept. This scheme is shown to be asymptotically stable using the convex control set (CCS) input constraint with space vector modulation or pulse width modulation and asymptotically set stable using the finite control set (FCS) input constraint (with direct actuation). The stability properties are guaranteed for any cost function that is globally defined and any prediction horizon $N \geq 1$. These results are validated using a software-in-the-loop (SiL) platform and an experimental test bench.**

***Index Terms*—Drive system, internal permanent-magnet synchronous motor, model predictive control (MPC), optimal control.**

I. Introduction

MODEL predictive control (MPC) is a control method for multidimensional nonlinear constrained systems that solves a constrained finite time optimal control (CFTOC) problem at each sampling time step. MPC has gained significant attention in drive systems research, where methods can be classified into model predictive current control (MPCC) [1], [2], model predictive torque control (MPTC) [3], [4], and model predictive speed control (MPSC) [5], [6]. Each can be combined with sensorless techniques [7], [8]. The methods can be further classified with respect to the switching behavior. Using a modulation scheme [space vector modulation (SVM), pulse width modulation (PWM)] yields convex control set (CCS) MPC [9], [10]. In finite control set (FCS) MPC [1], [11], switching states, i.e., voltage vectors, are actuated directly.

MPC needs to be executed in a real-time environment [12], [13]. The execution time is particularly critical for power electronics and drive systems, where sampling times are small and control code is executed on embedded hardware with mediocre computation power. Typically, the prediction horizon is chosen to be short (a few steps or $N = 1$) [1]–[6], [9], [10], [11], such that the CFTOC has a low dimension. This paper proposes to separate the permanent-magnet synchronous machine (PMSM) current–flux map (nonlinear or affine) from the dynamics, which is written in the $\alpha\beta$ flux space. This approach yields a simple dynamics (integrator) and time-invariant constraints. The resulting control scheme (Fig. 1) is capable of taking magnetic saturation and cross-saturation into account without affecting the control complexity. A torque controller is obtained combining the proposed method with a torque–current (or torque–flux) look-up table (LUT) or the constrained maximum torque per ampere (MTPA) concept [14].

The stability of MPC for drive systems is still an open research topic [15]. The MPC stability theorem [16]–[19] tends to be difficult to combine with controllers using an arbitrary cost function, a short prediction horizon, or solvers using early termination [20]–[22]. The MPC stability theorem (and derived concepts) uses the optimal cost function as a Lyapunov function between two sampling time instants (hence incompatible with early termination as it does not reveal the optimal cost at each sampling instant) [17]. This approach requires the system and constraints to be time-invariant and the predicted state sequence has to reach a terminal set. The terminal set needs to be control invariant and a control Lyapunov function (CLF) has to be satisfied for any state in set [17]. Either tends to be difficult to verify for an arbitrary cost function, e.g., with nonlinear components, and an integer input set. Also, the maximum control invariant set, i.e., the largest possible terminal set, can be small (dependent on the cost function). In this case, a long prediction horizon is necessary to cover a required set of initial states.

This paper proposes a uniform global and robust stability approach for CCS and FCS MPC. The resulting Lyapunov-based MPC uses a contraction constraint named CLF constraint to obtain stability. This constraint voids further requirements on the cost function (terminal cost and terminal set) or prediction horizon (generally a sufficiently long prediction horizon is required to achieve a sufficiently large feasible initial set, i.e., region of attraction). A major advantage of the proposed approach is the ability to choose an arbitrary cost function without affecting the stability properties of the closed-loop system (the cost function is typically the preferred tool to manipulate control behavior, e.g., the switching properties of FCS-MPC). Also, it can be shown that the stability properties are preserved in presence of early termination if the solution is primal feasible

Manuscript received June 16, 2015; revised November 21, 2015 and January 2, 2016; accepted January 14, 2016. Date of publication February 11, 2016; date of current version May 10, 2016.

The author is with the Department of Electrical Engineering, Columbia University in the City of New York, New York, NY 10027 USA (e-mail: matthias.preindl@columbia.edu).

Color versions of one or more of the figures in this paper are available online at http://ieeexplore.ieee.org.

Digital Object Identifier 10.1109/TIE.2016.2527722

0278-0046 © 2016 IEEE. Personal use is permitted, but republication/redistribution requires IEEE permission.
See http://www.ieee.org/publications_standards/publications/rights/index.html for more information.

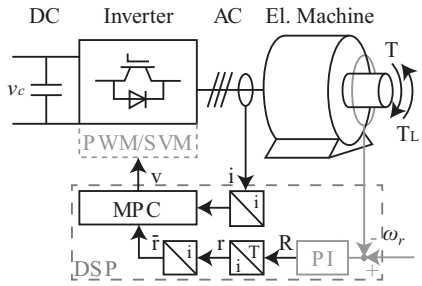

Fig. 1. Block diagram of MPC in the stator flux space; states: current i, flux λ; inputs: voltage v; references: flux $\bar{r}$, current r, torque R; the PWM/SVM block is used for CCS-MPC and removed for FCS-MPC; a proportional-integral (PI) controller is used for speed control and provides current references using the constrained MPTA concept [14].

TABLE I
NOMENCLATURE

Symbol	Description
$\mathbf{1}$	Vector of ones
$.^\dagger$	Moore–Penrose pseudoinverse
$\|.\|$ and $\|.\|_p$	Euclidean and p norm
$\circ$	Convolution
∂ and int	Boundary and interior of a set
$\oplus$ and $\ominus$	Minkowski sum and Pontryagin difference [23]
$\cap$ and $\cup$	Intersection and union of sets
$\mathbb{N}$, $\mathbb{N}_{\geq 0}$, $\mathbb{N}_{>0}$	Integers, nonnegative, and positive integers
$\mathbb{R}$, $\mathbb{R}_{\geq 0}$, $\mathbb{R}_{>0}$	Real, nonnegative, and positive real numbers
$\emptyset$	Empty set
$v_{\alpha\beta}$ and v_{dq}	Terminal voltage in $\alpha\beta$ and dq space
$i_{\alpha\beta}$ and i_{dq}	Stator current in $\alpha\beta$ and dq space
$\lambda_{\alpha\beta}$ and λ_{dq}	Flux linkage in $\alpha\beta$ and dq space
$\mathbf{T}_{\alpha\beta}$, $\mathbf{T}_{dq}(\epsilon)$	Clarke and Park transformation
ϵ and ω	Electrical rotor position and speed
$l(.)$	Nonlinear function mapping i_{dq} to λ_{dq}
$\mathbf{L}$ and ψ_{dq}	Inductance matrix and PM flux vector
$\mathcal{V}$, $\mathcal{V}_s$, and $\mathcal{V}_d$	Terminal voltage constraint set, FCS, and CCS
$\mathcal{O}(.)$	Preset [24], [17]

[25]. Robustness is achieved exploiting the voltage safety factor that is used in drive systems to ensure controllability [14]. The robust convergence of Lyapunov-based MPC is shown experimentally using a cost function that does not penalize the control errors but the variation of the input, i.e., switching.

This paper is organized as follows. The system model and constraints are introduced in Sections II and III, respectively; the stabilizability of the FCS system is shown in Section IV and is extended to the CCS system in Section V; the Lyapunov-based MPC is presented in Section VI and the validation is shown in Section VII. The notation of this paper is summarized in Table I.

II. Dynamic Model

The stator flux $\lambda_{\alpha\beta}(t) \in \mathbb{R}^2$ of a PMSM motor evolves according to [14], [25]

$$\lambda^+_{\alpha\beta} = \lambda_{\alpha\beta} + T_s v_{\alpha\beta} \tag{1}$$

where $\lambda_{\alpha\beta}$ is the flux in the $\alpha\beta$ reference frame, $\lambda^+_{\alpha\beta}$ is the flux of the next sampling time, and $v_{\alpha\beta} = v_{\alpha\beta,\text{termial}} - R_s i_{\alpha\beta}$ is the compensated terminal voltage. For notational simplicity, this equation is normalized dividing by the parameter $\Lambda_r = T_s v_c$

$$\bar{\lambda}^+_{\alpha\beta} = \bar{\lambda}_{\alpha\beta} + \bar{v}_{\alpha\beta} \tag{2}$$

where $\bar{\lambda}_{\alpha\beta} = \Lambda_r^{-1}\lambda_{\alpha\beta}$ is the normalized flux and $\bar{v}_{\alpha\beta} = v_c^{-1}v_{\alpha\beta}$ is the normalized compensated voltage. An $\boldsymbol{\alpha\beta}$ vector (current, voltage, flux) $z_{\alpha\beta}$ can be transformed into the dq reference frame with $z_{dq} = \mathbf{T}_{dq}(\epsilon)z_{\alpha\beta}$ using the Park transformation

$$\mathbf{T}_{dq}(\epsilon) = \begin{bmatrix} \cos\epsilon & \sin\epsilon \\ -\sin\epsilon & \cos\epsilon \end{bmatrix} \tag{3}$$

where ϵ is the electrical rotor position, which is either measured or estimated. In dq, the stator flux and armature (stator) currents are related by a static map in the dq reference frame equation [14], [25]

$$\lambda_{dq} = l \circ i_{dq} \approx \mathbf{L} i_{dq} + \psi_{dq} \tag{4}$$

where $l : \mathbb{R}^2 \to \mathbb{R}^2$ is the nonlinear current–flux relationship that takes saturation into account. It maps dq current into dq flux globally and can be computed via finite-element method (FEM) or measured experimentally. The map l is generally assumed to be invertible. For control purposes, this relation is often approximated with an affine equation using the parameters

$$\mathbf{L} = \begin{bmatrix} L_d & 0 \\ 0 & L_q \end{bmatrix}; \quad \psi_{dq} = \begin{bmatrix} \psi \\ 0 \end{bmatrix} \tag{5}$$

where L_d and L_q are the d - and q -axis inductance; ψ is the PM flux. This affine approximation is the basis for deriving the well-known dynamic model of anisotropic PMSM, which is written in the dq frame. However, the affine approximation can deviate significantly from the real flux–current relationship. A more general model is obtained interpreting (4) as (nonlinear) output function [25]

$$i_{\alpha\beta} = \mathbf{T}_{dq}^{-1}(\epsilon)\,(l^{-1} \circ (\mathbf{T}_{dq}(\epsilon)\lambda_{\alpha\beta})). \tag{6}$$

Since the map l is assumed to be bijective, a controller can be designed in the flux space and based on the time-invariant dynamics (2) without loss of generality. This approach yields the control system layout shown in Fig. 1. Using the PMSM stator flux as state comes with several benefits. The machine can be described using a linear or nonlinear (e.g., via LUT) current–flux relationship. This approach yields a simple dynamic model (integrator) that simplifies the formulation and prediction of MPC. The PMSM can be described either in the $\alpha\beta$ or dq flux space. In dq, the state (flux) is backward rotating while a control (flux) reference has to be forward rotating in $\alpha\beta$. In this research, the latter one is chosen since it yields nonrotating input constraints (see Section III) that are simpler to handle and more efficient to compute. In dq, the state has a parametric dependence on ω.

The goal of a current, i.e., flux, controller is to track a (normalized) flux reference vector $\bar{r}_{\alpha\beta} = \mathbf{T}_{dq}^{-1}(\epsilon)\bar{r}_{dq}$ that is applied externally, e.g., by a speed controller. Introducing the control

error $x = \bar{\lambda}_{\alpha\beta} - \bar{r}_{\alpha\beta}$, the tracking problem is transformed into a regulation problem that yields the state-space system

$$x^+ = x + u \tag{7}$$

and the input $u = \bar{v}_{\alpha\beta} - \bar{u}$ with

$$\bar{u} = -(\bar{r}_{\alpha\beta} - \bar{r}^+_{\alpha\beta}). \tag{8}$$

Thus, the normalized terminal voltage $\bar{v}_{\alpha\beta}$ is the sum of a *feedback* controller u, which depends on the control error, and a *feedforward* controller $\bar{u}$, which depends only on the reference. The feedback controller u is used to achieve desired closed-loop control properties, e.g., stability. The feedforward controller (8) is necessary to introduce a time-varying reference vector into the linear error dynamics (7). This controller can be simplified making typical assumptions on the drive system: the electrical speed is slowly varying with respect to T_s (zero order hold), i.e., the angle evolves according to $\epsilon^+ = \epsilon + T_s\omega$; and the dq flux reference vector is slowly varying with respect to T_s, i.e., $\bar{r}^+_{dq} \approx \bar{r}_{dq}$. Using these assumptions, $\bar{r}_{\alpha\beta}$ evolves according to [25]

$$\bar{r}^+_{\alpha\beta} \approx \mathbf{T}^{-1}_{dq}(\epsilon + T_s\omega)\mathbf{T}_{dq}(\epsilon)\bar{r}_{\alpha\beta} = \mathbf{T}^{-1}_{dq}(T_s\omega)\bar{r}_{\alpha\beta}. \tag{9}$$

This model describes $\bar{r}_{\alpha\beta}$ as a vector that rotates with velocity ω and by the angle $T_s\omega$ at each time step. Substituting this model into (8), a *proper* formulation for the feedforward controller is obtained

$$\bar{u} \approx -(\mathbf{I} - \mathbf{T}^{-1}_{dq}(T_s\omega))\bar{r}_{\alpha\beta} \tag{10}$$

that describes $\bar{u}$ as a function of $\bar{r}_{\alpha\beta}$ and the parameter ω.

III. System Constraints

A drive system cannot be operated with arbitrarily large states and inputs due to physical constraints. State constraints are introduced by the rated current limit that prevents semiconductors and the machine from overheating and failing. This is achieved limiting the current magnitude to $\|i\| \leq I_r$ where $I_r \in \mathbb{R}_{>0}$ is the rated current. However, limited transient violations (overshoots) are acceptable in most cases and it is sufficient that the reference value satisfies the state constraint. Thus, state limits are neglected for the MPC design and the stability assessment. If state constraints are required, they can be introduced as soft constraints.

On the other hand, input (voltage) limits need to be taken into account since voltage source inverters provide a voltage with finite magnitude. In this research, inverters are considered that apply the input $\bar{v}_{\alpha\beta}$ by either selecting switching states (direct actuation) or via modulation (SVM/PWM). Thus, the feasible inputs are defined by an input constraint set

$$\bar{v}_{\alpha\beta} = u + \bar{u} \in \mathcal{V} \quad \Leftrightarrow \quad u \in \mathcal{U} \overset{\text{def}}{=} \mathcal{V} - \bar{u} \tag{11}$$

where $\mathcal{U}$ is the $-\bar{u}$ shifted set $\mathcal{V}$, as shown in Fig. 2. A voltage source inverter provides a finite amount of switching state combinations. Applying these switching states directly yields a finite number of voltages vectors $v_{\alpha\beta} \in \mathcal{V} = \mathcal{V}_s$ that can be

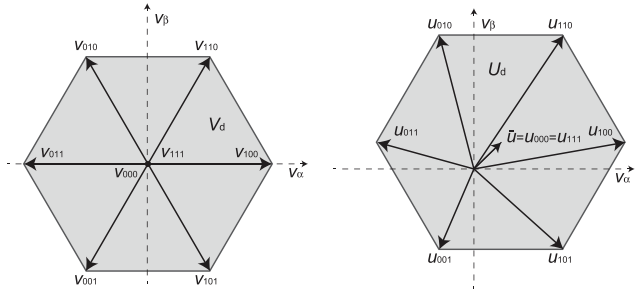

(a) Set $\mathcal{V}_s$ and $\mathcal{V}_d = \text{hull}\,\mathcal{V}_s$ (b) Set $\mathcal{U}_s$ and $\mathcal{U}_d = \text{hull}\,\mathcal{U}_s$

Fig 2. FCS and CCS input constraints.

applied to the terminals of an electrical machine. The set $\mathcal{V}_s$ is called FCS and is defined by

$$\mathcal{V}_s \overset{\text{def}}{=} \mathbf{T}_{\alpha\beta} \circ \{0,1\}^3 = \{v_{000}, v_{100}, \ldots, v_{111}\} \tag{12}$$

and $\mathcal{U}_s \overset{\text{def}}{=} \mathcal{V}_s - \bar{u}$ using the Clarke transformation

$$\mathbf{T}_{\alpha\beta} \overset{\text{def}}{=} \frac{2}{3}\begin{bmatrix} 1 & -1/2 & -1/2 \\ 0 & \sqrt{3}/2 & -\sqrt{3}/2 \end{bmatrix}. \tag{13}$$

These sets are depicted in Fig. 2. Using a modulation scheme (PWM/SVM), a combination of vectors can be applied such that any vector in the area spanned by $\mathcal{V}_s$ can be applied as input $v_{\alpha\beta} \in \mathcal{V} = \mathcal{V}_d$. The set $\mathcal{V}_d$ is called CCS and is defined as the convex hull of $\mathcal{V}_s$

$$\mathcal{V}_d \overset{\text{def}}{=} \text{hull}\mathcal{V}_s = \left\{ v \in \mathbb{R}^2 \mid \mathbf{H}v \leq \mathbf{1}/\sqrt{3} \right\} \tag{14}$$

and $\mathcal{U}_d \overset{\text{def}}{=} \mathcal{V}_d - \bar{u}$, where

$$\mathbf{H} \overset{\text{def}}{=} \begin{bmatrix} 0 & 1 \\ \sqrt{3}/2 & 1/2 \\ \sqrt{3}/2 & -1/2 \\ 0 & -1 \\ -\sqrt{3}/2 & -1/2 \\ -\sqrt{3}/2 & 1/2 \end{bmatrix}. \tag{15}$$

These sets are depicted in Fig. 2. The purpose of the input $u \in \mathcal{U}$ is to implement a stabilizing feedback. In general, this can be achieved if the origin belongs to the interior of $\mathcal{U}$, i.e., $0 \in \text{int}\mathcal{U}$. This is not practicable for $\mathcal{U}_s$ due to its integer nature. However, for the convex $\mathcal{U}_d$, it is obtained enforcing

$$\bar{u} \in \mathcal{V}_d \ominus \mathcal{B} = \left\{ v \in \mathbb{R}^2 \mid \mathbf{H}v \leq \frac{1}{\sqrt{3}} - b \right\} \tag{16}$$

where $b \in \left(0, \frac{1}{\sqrt{3}} - \|\mathbf{H}\bar{u}\|_\infty\right]$ and

$$\mathcal{B} \overset{\text{def}}{=} \left\{ v \in \mathbb{R}^2 \mid \mathbf{H}v \leq b \right\} \neq \emptyset. \tag{17}$$

This condition tends to $\bar{u} \in \text{int}\mathcal{V}_d$ as b tends to an infinitesimal value. The condition (16) limits the shift of $\mathcal{V}_d$ (by $-\bar{u}$) such that the resulting set $\mathcal{U}_d$ contains the origin in its interior. The condition on the feedforward controller $\bar{u}$ translates into a condition on the reference $\bar{r}_{\alpha\beta}$ (and ω).

Proposition 1: Let $|\,\omega\,|\,T_s\|\bar{r}_{\alpha\beta}\| = |\,\omega\,|\,T_s\|\bar{r}_{dq}\| < \frac{1}{\sqrt{3}} - b$, then $\bar{u} \in \mathcal{V}_d \ominus \mathcal{B}$.

Proof: Considering that the (inverse) Park transformation $\mathbf{T}_{dq}^{-1}(\epsilon)$ is orthogonal, i.e., $\|\bar{r}_{\alpha\beta}\| = \|\mathbf{T}_{dq}^{-1}(\epsilon)\bar{r}_{dq}\| = \|\bar{r}_{dq}\|$, it can be shown that $\|\bar{u}\|$ is upper bounded by $|\,\omega\,|\,T_s\|\bar{r}_{\alpha\beta}\| = |\,\omega\,|\,T_s\|\bar{r}_{dq}\|$, since

$$\|\bar{u}\| = \left\|-(\mathbf{I} - \mathbf{T}_{dq}^{-1}(\omega T_s))\bar{r}_{\alpha\beta}\right\| \leq |\,\omega\,|\,T_s\|\bar{r}_{\alpha\beta}\| \tag{18a}$$

$$1 - (\omega T_s)^2/2 \leq \cos\omega T_s \tag{18b}$$

is always true. Thus, the condition

$$\|\bar{u}\| \leq |\,\omega\,|\,T_s\|\bar{r}_{\alpha\beta}\| = |\,\omega\,|\,\|\bar{r}_{dq}\| < 1/\sqrt{3} - b \tag{19}$$

implies $\|\bar{u}\| < 1/\sqrt{3} - b \Leftrightarrow \bar{u} \in \text{ball}(\mathcal{V}_d \ominus \mathcal{B}) \subset \mathcal{V}_d \ominus \mathcal{B}$, where ball denotes the Chebyshev ball. ■

This result formalizes that a reference vector needs to satisfy the well-known voltage, i.e. flux constraint $|\omega|\,\|r_{dq}\| < (\frac{1}{\sqrt{3}} - b)v_c$ at all time. A small robustness parameter b is typically used to prevent the system form attempting to operate on or beyond the voltage limit due to model uncertainties [4], [14]. The voltage constraint is typically satisfied at low speed but it implies that field weakening is required to operate a machine at high speeds.

IV. Constrained Stabilizability With FCS

Using the FCS input constraints, the closed-loop system *cannot* converge to the origin in general. Since the FCS is an integer input set, there exists a limit how close state x can be driven toward the origin by feasible inputs $u \in \mathcal{U}_s$. In other words, a Lyapunov function value cannot be decreased beyond a certain value. Thus, the closed-loop system is set stable at best. Set stability means that the state converges to a set $\mathcal{D}$ containing the origin, where it remains ultimately bounded. The set stabilizability of the FCS system is analyzed using the candidate CLF

$$\Gamma(x) \stackrel{\text{def}}{=} \|\mathbf{H}x\|_\infty \tag{20}$$

where $\mathbf{H}$ is defined in (15). The candidate CLF $\Gamma(x)$ is positive definite and radially unbounded. This function has hexagonal sublevel sets

$$\Omega(\gamma) = \left\{u \in \mathbb{R}^2 \mid \mathbf{H}x \leq \gamma\right\} \tag{21}$$

which are *similar* to (14). Let us now introduce the concept of *preset* [17], [24] to derive system properties.

Definition 1: The *preset* $\mathcal{O}(\Omega(\gamma)) \subset \mathbb{R}^2$ is the set of states $x \in \mathbb{R}^2$ which can be driven by an admissible control input $u \in \mathcal{U}_s$ to the set $\Omega(\gamma) \subset \mathbb{R}^2$, i.e.,

$$\mathcal{O}(\Omega(\gamma)) \stackrel{\text{def}}{=} \left\{x \in \mathbb{R}^2 \mid \exists u \in \mathcal{U}_s : x + u \in \Omega(\gamma)\right\}. \tag{22}$$

The preset can be computed for the sublevel set $\Omega(\gamma)$ and the dynamics (7) according to Definition 1

$$\begin{aligned}\mathcal{O}(\Omega(\gamma)) &= \left\{x \in \mathbb{R}^2 \mid \exists u \in \mathcal{U}_s : x + u \in \Omega(\gamma)\right\}\\ &= \left\{x \in \mathbb{R}^2 \mid \exists y \in \Omega(\gamma),\ \exists u \in \mathcal{U}_s : x = y - u\right\}\\ &= \Omega(\gamma) \oplus (-\mathcal{U}_s).\end{aligned} \tag{23}$$

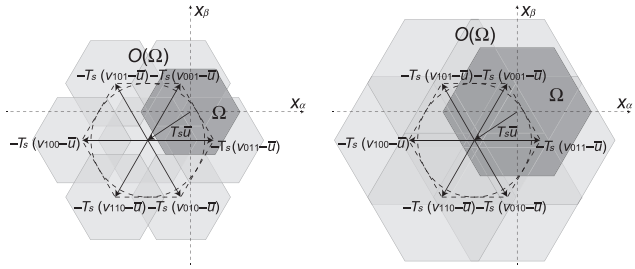

(a) $\Omega(\gamma)$ with $\gamma < \frac{1}{\sqrt{3}}$ (b) $\Omega(\gamma)$ with $\gamma \geq \frac{1}{\sqrt{3}}$

Fig. 3. Preset $\mathcal{O}(\Omega(\gamma))$.

A useful interpretation of the Minkowski sum $\oplus$ is that it is the union of all translated copies of $\Omega(\gamma)$ by the vectors of $(-\mathcal{U}_s)$ [23]

$$\mathcal{O}(\Omega(\gamma)) = \bigcup_{u_{\iota\iota\iota} \in \mathcal{U}_s} (\Omega(\gamma) - u_{\iota\iota\iota}) = \bigcup_{v_{\iota\iota\iota} \in \mathcal{V}_s} (\Omega(\gamma) - v_{\iota\iota\iota}) + \bar{u}.$$

Thus, the preset is the union of $2^3 = 8$ polytopes, which is shown in Fig. 3. The properties of this set depend on the size of $\Omega(\gamma)$. It is noted that the vectors $\boldsymbol{v}_{100}, \ldots, \boldsymbol{v}_{011}$ have length $2/3$ due to the normalization with Λ_r in (7). If $\gamma < \frac{1}{\sqrt{3}}$, then $\mathcal{O}(\Omega(\gamma))$ is nonconvex, which is portrayed in Fig. 3(a). If γ is further reduced, then the polytopes forming $\mathcal{O}(\Omega(\gamma))$ are not even connected. If $\gamma \geq \frac{1}{\sqrt{3}}$, then adjacent polytopes forming $\mathcal{O}(\Omega(\gamma))$ overlap such that the resulting $\mathcal{O}(\Omega(\gamma))$ is convex. This case is shown in Fig. 3(b) and the resulting set is described by

$$\begin{aligned}\mathcal{O}(\Omega(\gamma)) &= \left\{x \in \mathbb{R}^2 \mid \mathbf{H}x \leq \gamma + \frac{1}{\sqrt{3}}\right\} + \bar{u}\\ &= \Omega(\gamma) \oplus (-\mathcal{V}_d) + \bar{u} = \Omega(\gamma) \oplus (-\mathcal{U}_d).\end{aligned} \tag{24}$$

Thus, the following result can be obtained.

Proposition 2: Let $\bar{u} \in \mathcal{V}_d \ominus \mathcal{B}$ and $u \in \mathcal{U}_s$ then $\Omega(\gamma) \oplus \mathcal{B} \subset \mathcal{O}(\Omega(\gamma))$ for all $\gamma \geq \frac{1}{\sqrt{3}}$.

Proof: First, let us find the largest set Υ that is always contained in the preset

$$\Upsilon \subset \mathcal{O}(\Omega(\gamma)) \quad \forall \bar{u} \in \mathcal{V}_d \ominus \mathcal{B} \tag{25}$$

where the size of $\mathcal{B}$ is defined by $b \in \left(0, \frac{1}{\sqrt{3}} - \Gamma(\bar{u})\right]$. If $\gamma \geq \frac{1}{\sqrt{3}}$, then $\mathcal{O}(\Omega(\gamma)) = \Omega(\gamma) \oplus (-\mathcal{V}_d) + \bar{u}$ according to (24). Hence, Υ can be written as the intersection of all translated copies

$$\Upsilon = \bigcap_{\bar{u} \in \mathcal{V}_d \ominus \mathcal{B}} (\Omega(\gamma) \oplus (-\mathcal{V}_d) + \bar{u}) \tag{26}$$

which is known as the Pontryagin (Minkowski) difference [23]

$$\Upsilon = (\Omega(\gamma) \oplus (-\mathcal{V}_d)) \ominus (\mathcal{V}_d \ominus \mathcal{B}). \tag{27}$$

Due to the specific structure of these sets we obtain

$$\Upsilon = \left\{u \in \mathbb{R}^2 \mid \mathbf{H}u \leq \gamma + \frac{1}{\sqrt{3}} - \left(\frac{1}{\sqrt{3}} - b\right)\right\} \tag{28}$$

or $\Upsilon = \Omega(\gamma) \oplus \mathcal{B}$ and we conclude $\Omega(\gamma) \oplus \mathcal{B} \subset \mathcal{O}(\Omega(\gamma))$. ■

Thus, any sublevel set $\Omega(\gamma)$ with $\gamma \geq \frac{1}{\sqrt{3}}$ belongs to the strict interior of its preset $\mathcal{O}(\Omega(\gamma))$ with some robustness margin (if $\bar{u} \in \mathcal{V}_d \ominus \mathcal{B}$). If $\gamma < \frac{1}{\sqrt{3}}$, this properties do not hold in general, which is shown in Fig. 3(a). Proposition 2 can be used to derive a CLF [26].

Proposition 3: Let $\bar{u} \in \mathcal{V}_d \ominus \mathcal{B}$ then $\exists u \in \mathcal{U}_s$ such that

$$\Gamma(x+u) - \max\left(\Gamma(x), \frac{1}{\sqrt{3}} + b\right) \leq -b. \tag{29}$$

Proof: Let $\bar{u} \in \mathcal{V}_d \ominus \mathcal{B}$. The set $\Omega(\frac{1}{\sqrt{3}}) = \mathcal{V}_d$ is control invariant [17] since $\mathcal{V}_d \subseteq \mathcal{O}(\mathcal{V}_d)$. Thus, for every $x \in V_d$ exists a admissible input such that $x + u \in \mathcal{V}_d$, i.e., $\exists u \in \mathcal{U}_s$

$$\Gamma(x+u) - 1/\sqrt{3} \leq 0 \;\; \forall x \in \mathcal{V}_d. \tag{30}$$

The Proposition 2 applies for larger sublevel sets $\Omega(\gamma) \supseteq V_d \oplus \mathcal{B}$. It implies we can find a set such that $x \in \partial(\Omega(\gamma) \oplus \mathcal{B})$ and an admissible input exists such that $x + u \in \Omega(\gamma)$. Hence, there $\exists u \in \mathcal{U}_s$ such that

$$\Gamma(x+u) - \Gamma(x) < -b \quad \forall x \in \mathbb{R}^2 \setminus \mathcal{V}_d. \tag{31}$$

Any state $x \in (V_d \oplus \mathcal{B}) \setminus V_d$ can be steered to V_d but typically not with the $-b$ margin, which yields (29). ■

According to Proposition 3, the value of a candidate CLF can be decreased robustly for all $x \in \mathbb{R}^2 \setminus \mathcal{V}_d$. Thus, any state $x \in \mathbb{R}^2 \setminus \mathcal{V}_d$ can be steered toward the set $\mathcal{V}_d$. Moreover, for all $x \in \mathcal{V}_d$ there exists an $u \in \mathcal{U}_s$ such that $x + u \in \mathcal{V}_d$. As a consequence, there exists a sequence $u(0), u(T_s), \ldots, u(kT_s), \ldots \in \mathcal{U}_s$ such that

$$\lim_{k\to\infty} x(kT_s) \in \mathcal{D} \stackrel{\text{def}}{=} \mathcal{V}_d \tag{32}$$

and the FCS system is said to be *global and robust asymptotically set stabilizable*. An illustration of CLF sublevel sets and their presets is shown Fig. 4.

Choosing the robustness parameter, i.e., limiting $\bar{u} \in \mathcal{V}_d \ominus \mathcal{B} \subset \text{int}\mathcal{V}_d$, is a design decision. According to Proposition 1, $\bar{u}$ is a rotating vector that needs to satisfy the voltage limit $|\omega| \, \|r_{dq}\| < \frac{v_c}{\sqrt{3}}$. Increasing b requires field weakening to start earlier and reduces the available maximum torque at high-speed operation. Hence, choosing b is a trade-off between robust convergence and exploiting the maximum terminal voltage at high-speed operation. However, field weakening algorithms also maintain a voltage margin due to robustness considerations in practice [14]. This margin can be used to choose b. Optionally, robustness can be maximized using a variable b, e.g., using different values for low- and high-speed operation or choose it according to its maximum $b = \frac{1}{\sqrt{3}} - \Gamma(\bar{u})$.

V. Constrained Stabilizability With CCS

The CCS input constraint is a superset of the FCS, i.e., $\mathcal{U}_s \subset \mathcal{U}_d$. Hence, the CCS system inherits the stability properties of the FCS system. However, the CCS system is able to converge

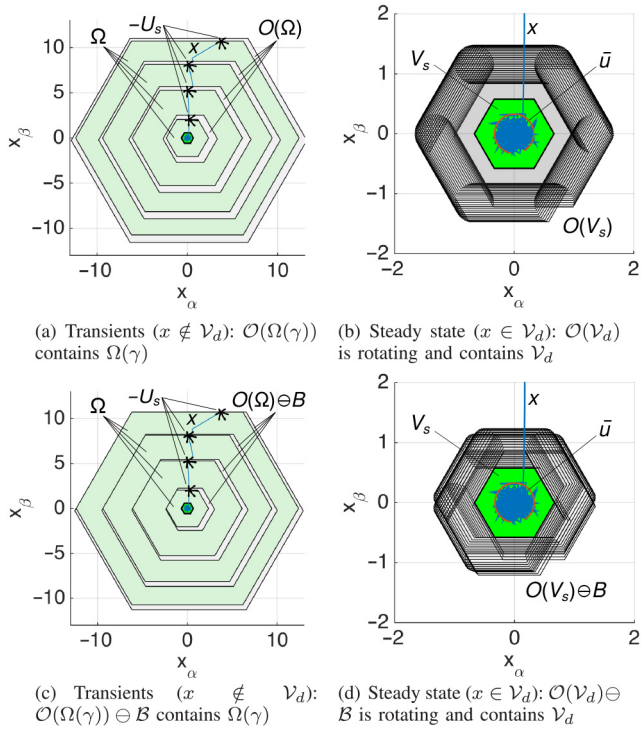

(a) Transients ($x \notin \mathcal{V}_d$): $\mathcal{O}(\Omega(\gamma))$ contains $\Omega(\gamma)$

(b) Steady state ($x \in \mathcal{V}_d$): $\mathcal{O}(\mathcal{V}_d)$ is rotating and contains $\mathcal{V}_d$

(c) Transients ($x \notin \mathcal{V}_d$): $\mathcal{O}(\Omega(\gamma)) \ominus \mathcal{B}$ contains $\Omega(\gamma)$

(d) Steady state ($x \in \mathcal{V}_d$): $\mathcal{O}(\mathcal{V}_d) \ominus \mathcal{B}$ is rotating and contains $\mathcal{V}_d$

Fig. 4. FCS-MPC candidate CLF applying a positive torque step of 1 pu at 0.5 pu speed: (top) presets $\mathcal{O}(\Omega(\gamma))$ with infinitesimal b; and (bottom) *robust* presets $\mathcal{O}(\Omega(\gamma)) \ominus \mathcal{B}$ with largest admissible $\mathcal{B}$ defined by $b = \frac{1}{\sqrt{3}} - \Gamma(\bar{u})$.

to the origin and stronger stability properties can be derived. The CCS preset is defined according to Definition 1

$$\mathcal{O}(\Omega(\gamma)) = \Omega(\gamma) \oplus (-\mathcal{U}_d). \tag{33}$$

Hence, the following can be said.

Proposition 4: Let $\bar{u} \in \mathcal{V}_d \ominus \mathcal{B}$ and $u \in \mathcal{U}_d$ then $\Omega(\gamma) \oplus \mathcal{B} \subset \mathcal{O}(\Omega(\gamma))$ for all $\gamma \geq 0$.

Proof: The proof is similar to the proof of Proposition 2 considering (33). ■

For CCS, any sublevel set $\Omega(\gamma)$ with $\gamma \geq 0$ belongs to the strict interior of its preset $\mathcal{O}(\Omega(\gamma))$ with some robustness margin (if $\bar{u} \in \mathcal{V}_d \ominus \mathcal{B}$). Thus, a CLF can be defined with extended stability properties at the origin.

Proposition 5: Let $\bar{u} \in \mathcal{V}_d \ominus \mathcal{B}$ then $\exists u \in \mathcal{U}$ such that

$$\Gamma(x+u) - \max\left(\Gamma(x), b\right) \leq -b. \tag{34}$$

Proof: The proof is similar to the proof of Proposition 3 considering Proposition 33. ■

According to Proposition 5, the value of a candidate CLF can be decreased robustly for all $x \in \mathbb{R}^2$. Thus, any state $x \in \mathbb{R}^2$ can be steered toward the origin and there exists a sequence $u(0), u(T_s), \ldots, u(kT_s), \ldots \in \mathcal{U}_d$ such that

$$\lim_{k\to\infty} x(kT_s) = 0 \tag{35}$$

and the CCS system is said to be *global and robust asymptotically stabilizable*.

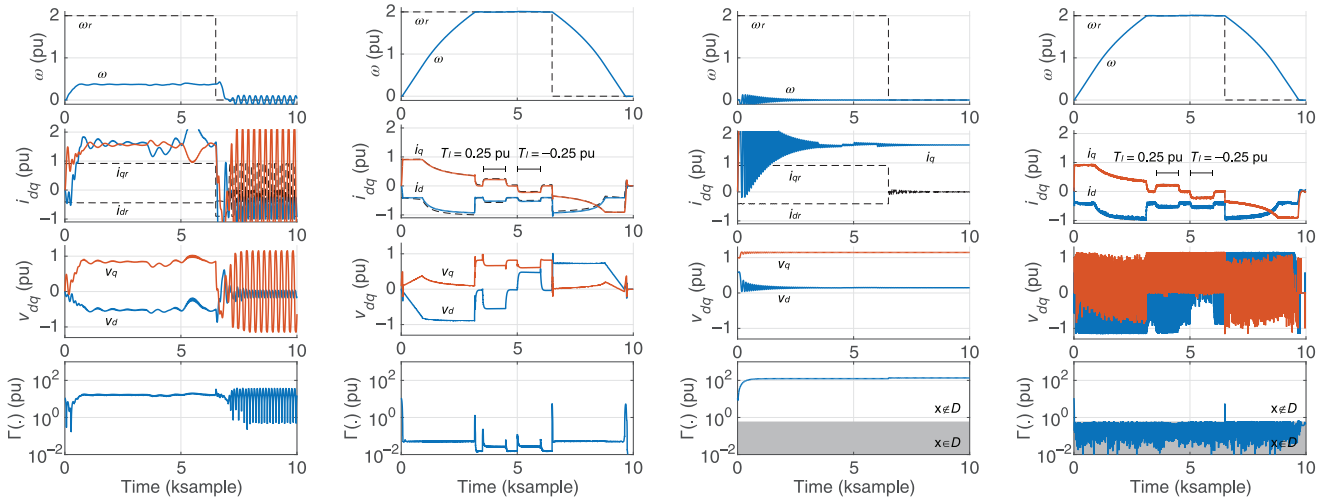

(a) CCS-MPC without CLF (b) CCS-MPC with CLF (c) FCS-MPC without CLF (d) FCS-MPC with CLF

Fig. 5. Software in the Loop (SiL) validation: MPC using the cost function (38) with horizon $N = 4$ and tuning parameter $q = 10^{-2}$ (heavy penalization of input variations, i.e., switching) applying a 2 pu (field weakening) speed steps and ± 0.25 pu load torque steps; curves: speed ω, current i_{dq}, voltage v_{dq}; Lyapunov function $\Gamma(\cdot)$; speed and current reference values are dashed.

It is noted that the CCS system is compatible also with different Lyapunov functions, e.g., $\|x\|_g$ with $g \in \{1, 2, \infty\}$ [25]. However, they cannot be used with FCS and are not omitted due to shortness.

VI. Model Predictive Control

MPC is defined by the CFTOC problem [17]. Considering the Lyapunov-based MPC approach [27], [28], the following CFTOC is defined

$$\underset{u_0,\ldots,u_{N-1}}{\text{minimize}}\ J(\cdot) \tag{36a}$$

$$\text{subject to } x_{j+1} = x_j + u_j \tag{36b}$$

$$u_j \in \mathcal{U}_j \stackrel{\text{def}}{=} \mathcal{V} - \bar{u}_j \tag{36d}$$

$$\Gamma(x_0 + u_0) - \max\left(\Gamma(x_0), \bar{\gamma} + b\right) \leq -b \tag{36d}$$

where $\bar{\gamma} = \frac{1}{\sqrt{3}}$ for FCS; $\bar{\gamma} = 0$ for CCS; and $b \in (0, \frac{1}{\sqrt{3}} - \Gamma(\bar{u})]$. The CLF constraint (36d) requires the first input u_0 to be stabilizing. Optionally, this constraint can be modified such that the entire input u_j sequence is stabilizing.

The *cost function* (36a) defines the control goals taking $N \in \mathbb{N}_{>0}$ future time steps into account, which is called the *prediction horizon*. It is assumed to be globally defined and does not impose hard constraints (e.g., barrier functions [29]). The cost function is minimized taking *constraints* into account. The optimization problem satisfies the plant dynamic due to (36b), which is parametrized with the state measurement $x_0 = x$. The input constraints are taken into account by (36c), which is parametrized by the sequence $\bar{u}_0, \ldots, \bar{u}_{N-1}$. The notation $.j$ is introduced for the open-loop predictions at a give sampling instant with $j \in \{0, \ldots, N\}$.

The CFTOC (36) is solved by an input $\mathrm{U} \stackrel{\text{def}}{=} [u_0', \ldots, u_{N-1}']'$ and state sequence $\mathrm{X} \stackrel{\text{def}}{=} [x_1', \ldots, x_N']'$ that are said to be *feasible*, if they satisfy the CFTOC constraints. Moreover, $\mathrm{U}^\star$ and $\mathrm{X}^\star$ are the *optimal* sequences that yield $J(x_0, \mathrm{U}^\star) \leq J(x_0, \mathrm{U})$ for all feasible U. Thus, the CFTOC (36) is said to be feasible if at least one feasible sequence U and X can be found. Moreover, it is said to be *persistently feasible* if it is feasible for all future time steps.

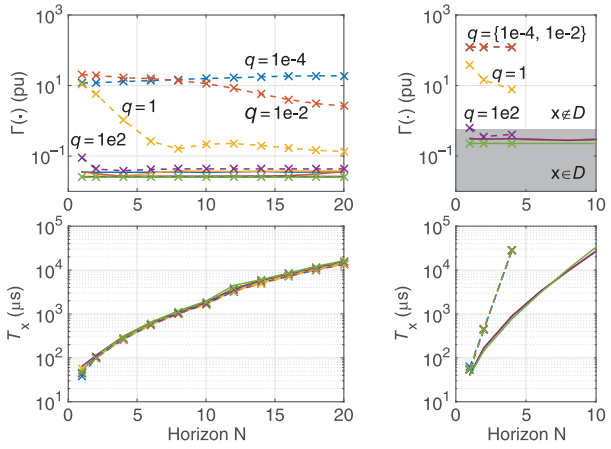

(a) CCS-MPC (b) FCS-MPC

Fig. 6. Software-in-the-loop (SiL) validation: MPC with (solid) and without (dashed with markers) CLF constraint using the cost function (38): Lyapunov function $\Gamma(\cdot)$ and execution time T_x mean values obtained from testing conditions in Fig. 5.

Proposition 6: If $\bar{u}_j \in \mathcal{V}_d \ominus \mathcal{B}$, then the CFTOC (36) is feasible for all $x_0 \in \mathbb{R}^2$.

Proof: If $\bar{u}_j \in \mathcal{V}_d \ominus \mathcal{B}$, then an input $u_j \in \mathcal{U}_j$ exists that satisfies (36b), (36c), and (36d) due to Proposition 3 (for FCS) and Proposition 5 (for CCS). ■

The CFTOC (36) is parametrized by the sequence $\bar{u}_0, \ldots, \bar{u}_{N-1}$ (in addition to x_0). However, the evolution of $\bar{u}$, i.e., $\bar{r}_{dq}$ and ω, is rarely available and typically approximated with constant sequences [30], [31]

$$\bar{u}_j \approx -\left(\mathbf{I} - \mathbf{T}_{dq}^{-1}(\omega_0 T_s)\right)\mathbf{T}_{dq}^{-1}(\epsilon + j\omega_0 T_s)\bar{r}_{dq,0}. \tag{37}$$

In this case, the Proposition 6 simplifies as follows.

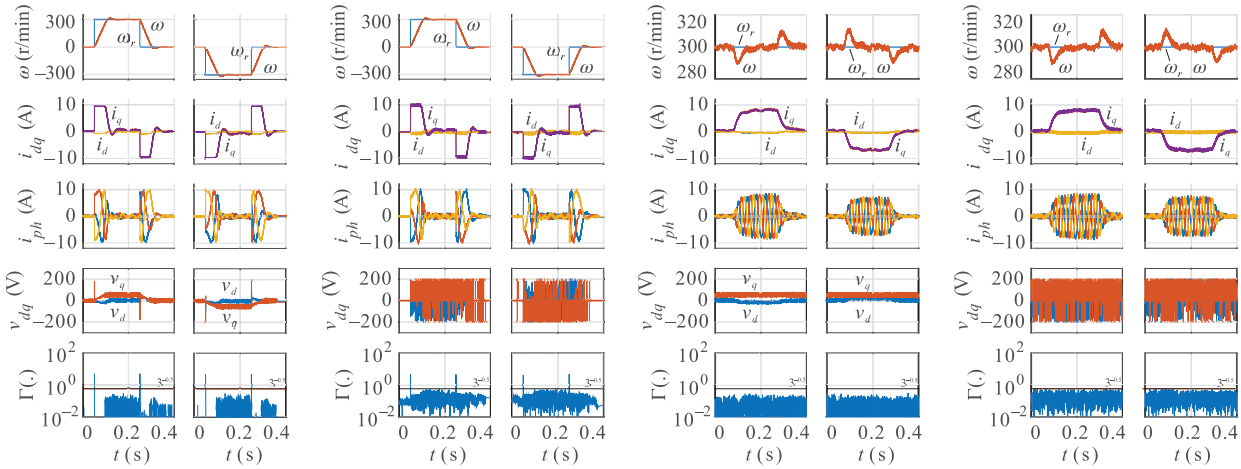

(a) CCS-MPC speed steps (b) FCS-MPC speed steps (c) CCS-MPC torque steps (d) FCS-MPC torque steps

Fig. 7. Experimental validation: (left) 300 r/min speed steps and (right) 20 Nm load torque steps using MPC with CLF and cost function (38) with horizon $N = 2$ and tuning parameter $q = 0$; curves: speed ω, current i_{dq}, flux λ_{dq}; Lyapunov function $\Gamma(\cdot)$.

Corollary 1: Let $\omega_0 = \cdots = \omega_N$ and $\bar{r}_{dq,0} = \cdots = \bar{r}_{dq,N}$ and $\bar{u}_0 \in \text{ball}(\mathcal{V}_d \ominus \mathcal{B})$, then the CFTOC (36) is feasible for all $x_0 \in \mathbb{R}^2$.

Proof: If ω_j and $\bar{r}_{dq,j}$ are constant, then $\|\bar{r}_{\alpha\beta,j}\|$ and $\|\bar{u}_j\|$ are constant. Thus, $\bar{u}_0 \in \text{ball}(\mathcal{V}_d \ominus \mathcal{B})$ implies $\bar{u}_j \in \text{ball}(\mathcal{V}_d \ominus \mathcal{B})$ for all $j \in [0, N]$ and Propositions 6 holds. ■

MPC computes $\mathrm{U}^\star$ at each time step. Then, the first of the optimal input is applied to the plant $u \stackrel{\text{def}}{=} u_0^\star$ and algorithm waits until the next sampling instant. This policy defines an implicit feedback control law, i.e., a closed-loop control system, that can be analyzed for stability.

Theorem 1: Let $\bar{u}_j \in \mathcal{V}_d \ominus \mathcal{B}$ for all future time steps, MPC solves the CFTOC (36) at each time step and applies $u(kT_s) = u_0^\star$ to the plant. Then, the resulting closed-loop system is global and robust asymptotically stable using $\mathcal{U} = \mathcal{U}_d$ (for CCS) and asymptotically set stable using $\mathcal{U} = \mathcal{U}_s$ (for FCS).

Proof: If $\bar{u}_j \in \mathcal{V}_d \ominus \mathcal{B}$ for all future time steps, the CFTOC (36) is persistently feasible and produces an optimal input sequence U. The first input satisfies the (candidate) CLF constraint (36d) and is applied to the plant. Hence, the closed-loop system inherits the stability properties of the CLF. ■

VII. Implementation and Results

Lyapunov-based MPC is implemented using the reference cost function (any other cost function can be used for validation) with delta input

$$J(\cdot) \stackrel{\text{def}}{=} \sum_{j=0}^{N-1} \left(x'_{j+1} \mathbf{Q} x_{j+1} + \Delta v'_j \mathbf{R} \Delta v_j \right) \tag{38}$$

where $\Delta \bar{v}_j = \bar{v}_j - \bar{v}_{j-1}$, which can be interpreted as a switching penalization for FCS (the subscript $._{\alpha\beta}$ is neglected for compactness). The components of x_j are the α and β flux error that are decoupled from each other and should be weighted with equivalent importance. Thus, the matrices are simplified as $\mathbf{Q} \stackrel{\text{def}}{=} q\mathbf{I}$ and $\mathbf{R} \stackrel{\text{def}}{=} \mathbf{I}$. The tuning parameter $q \in \mathbb{R}_{>0}$ can be interpreted as gain. Hence, the CFTOC (36) is rewritten in simplified form

$$\underset{v_0,\ldots,v_{N-1}}{\text{minimize}} \quad \sum_{j=0}^{N-1} \left(q x'_{j+1} x_{j+1} + \Delta v'_j \Delta v_j \right) \tag{39a}$$

$$\text{subject to} \quad \bar{\lambda}_{j+1} = \bar{\lambda}_j + \bar{v}_j \tag{39b}$$

$$x_j = \bar{\lambda}_j - \bar{r}_j;\ \bar{v}_j \in \mathcal{V} \tag{39c}$$

$$\Gamma(x_j) - \max\left(\Gamma(x_j), \bar{\gamma} + b\right) \leq -b. \tag{39d}$$

It can be shown that Lyapunov-based MPC yields also implementation benefits compared to standard MPC that are discussed under another cover for compactness [25].

To validate Lyapunov-based MPC, it is compared to MPC without CLF constraint. First, the concepts are tested on a SiL platform that allows us to precisely control initial conditions, sensor noise, and remove real-time constraints to investigate long horizons. In Fig. 5, results are shown using $q = 10^{-2}$ and $N = 4$. In these conditions, MPC without CLF does not converge but Lyapunov-based MPC provides satisfactory control performance. Lyapunov-based FCS-MPC satisfies the terminal constraint in steady-state conditions. As expected, the $\Gamma(\cdot)$ exceeds $\frac{1}{\sqrt{3}}$ only when a large reference step is applied. Lyapunov-based CCS-MPC yields a lower $\Gamma(\cdot)$ in general. However, the value is nonzero even in steady-state conditions due to simulated nonlinear behavior of the model (dead-times and sensor noise). The test has been repeated varying the tuning parameter $q = 10^{\{-2,1,2,4\}}$ and prediction horizon N. In Fig. 6, the mean values of $\Gamma(\cdot)$ and the execution time T_x are shown as a function of N. Lyapunov-based FCS-MPC can exploit the CLF constraint (applied to each prediction step) to optimize T_x [25].

MPC with and without CLF and prediction horizon $N = 2$ is combined with a delay observer [25] and implemented on the experimental IPM test bench with dSpace Microautobox II; dc-link voltage $v_c = 300$ V; rated current $I_r = 10$ Ap; and parameters: pole pairs $p = 5$, inductance $L_d = 10.5$ mH, $L_q = 12.9$ mH, PM flux $\psi = 342$ mWb, and shaft inertia $J = 8.7 \times 10^{-3}$ kg m^2. CCS-MPC is implemented as explicit MPC and results in a code execution time of 1.9 µs; FCS-MPC is implemented using an enumeration strategy that

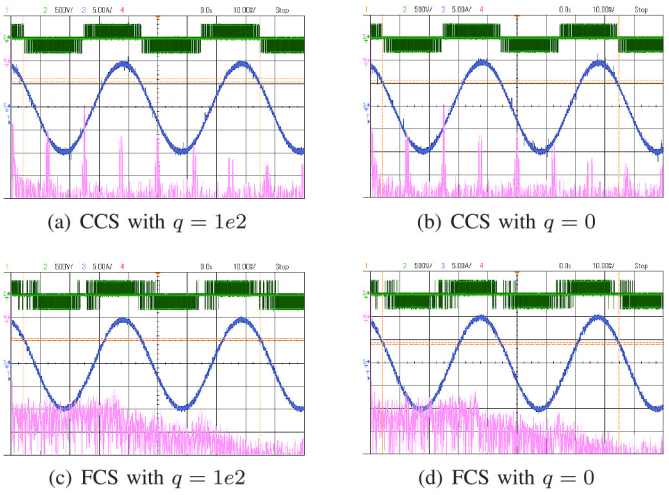

(a) CCS with $q = 1e2$ (b) CCS with $q = 0$

(c) FCS with $q = 1e2$ (d) FCS with $q = 0$

Fig. 8. Oscilloscope screenshot of MPC with CLF: line-to-line voltage, phase current, and current FFT (0 Hz to 20 kHz range) at switching frequency $f_{\mathrm{sw}} \approx 2.5$ kHz (sampling frequency $f_s = 5$ kHz for CCS-MPC and $f_s = 20$ kHz for FCS-MPC), dc-link voltage $v_c = 300$ V, rotational speed $n = 300$ r/min.

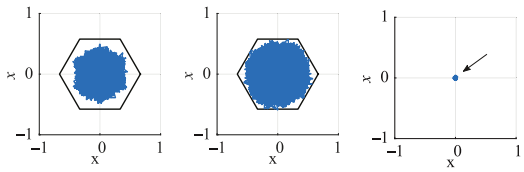

(a) FCS with $q = 1e2$ (b) FCS with $q = 0$ (c) CCS with $q = 0$

Fig. 9. Steady-state control error at switching frequency $f_{\mathrm{sw}} \approx 2.5$ kHz (sampling frequency $f_s = 5$ kHz for CCS-MPC and $f_s = 20$ kHz for FCS-MPC), dc-link voltage $v_c = 300$ V, rotational speed $n = 300$ r/min.

results in an execution time of 2.8 µs. Both execution times are given for MPC only, i.e., without considering speed control or sensor reading. The transient response of MPC with CLF constraint and $q = 0$ is validated applying 300 r/min positive and negative speed reference steps and 20 Nm load torque steps in Fig. 7 using a PI speed controller with clamping antisaturation technique. The results show the fast transient response expected by MPC and confirm the findings of the SiL evaluation showing the effectiveness of the robust CLF constraint. Choosing $q = 0$ means not penalizing the control error in the cost function and reference tracking is only performed by the CLF constraint. For obvious reasons, MPC without CLF cannot work in the same conditions. The steady-state performance of MPC with CLF constraint is shown in Figs. 8 and 9. Both FCS-MPC and CCS-MPC achieve approximately the same switching frequency and current ripple in both cases but differ in terms of current spectrum. CCS-MPC achieves the typical PWM harmonics while FCS-MPC has a more random ripple with approximately white noise spectrum. Using FCS-MPC with CLF, the error x is guaranteed to converge to $\mathcal{D} \stackrel{\mathrm{def}}{=} \mathcal{V}_d$ that is shown in Fig. 9(a) and (b). The error can converge to a subset of $\mathcal{D}$ for large q [see Fig. 9(a)] but this cannot be guaranteed in general. CCS-MPC converges to the origin as it is shown in Fig. 9(c) (CCS-MPC does not "see" the current ripple due to PWM).

Due to the formulation in the normalized flux space, the MPC formulation itself is parameter independent. However, the flux and flux reference are computed based on the current values using the current–flux relationship. Thus, the effect of

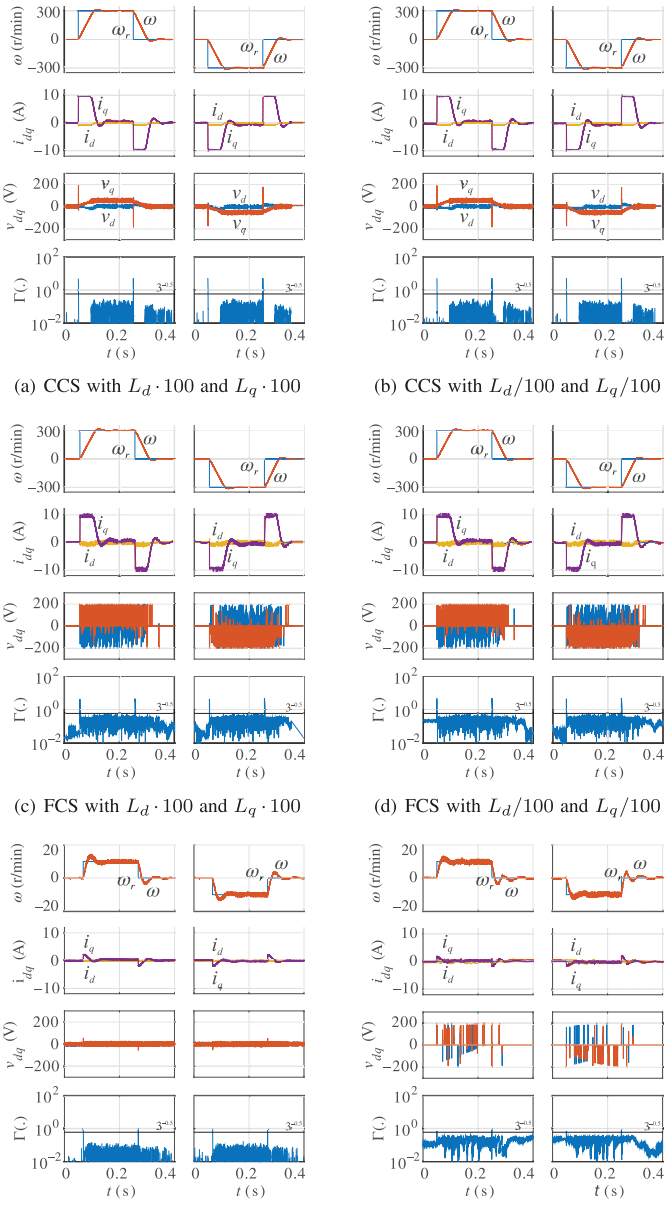

(a) CCS with $L_d \cdot 100$ and $L_q \cdot 100$ (b) CCS with $L_d/100$ and $L_q/100$

(c) FCS with $L_d \cdot 100$ and $L_q \cdot 100$ (d) FCS with $L_d/100$ and $L_q/100$

(e) CCS with $R_s = 0\Omega$ (f) FCS with $R_s = 0\Omega$

Fig. 10. Experimental validation of the parameter robustness of MPC with CLF constraint: over and underestimation of the machine inductance by a factor of 100 (300 r/min speed steps) and low-speed test neglecting phase resistance (10 r/min speed steps; encoder quantization is 0.75 r/min).

an inductance mismatch is evaluated in Fig. 10. It is shown that even a L_d and L_q mismatch by a factor of 100 has no significant effect on Lyapunov-based MPC. Similar results can be shown for ψ. The phase resistance was found to have a limited to no effect throughout simulation and was neglected during experimental testing. A low-speed test is shown in Fig. 10 where the resistive voltage drop is significant compared to the terminal voltage. Overcompensating the resistive voltage drop by a factor of 10 yields to a matching result (not shown due to compactness). Overcompensation beyond that factor can reverse the sign (or more generally the direction) of the terminal voltage at low speed (in CCS-MPC) and triggered overcurrent events during testing. Summarizing, the testing shows that the

proposed Lyapunov-based MPC is (sufficiently) robust. In practice, much better parameter knowledge is needed for MTPA tracking, field weakening, or sensorless control. It is further noted that Lyapunov-based MPC was validated for high-speed operation [14], where Lyapunov-based MPC is used to validate the constrained-MTPA concept.

VIII. Conclusion

This paper has proposed a novel Lyapunov-based MPC scheme for PMSM drive systems. The concept adds a CLF constraint and the resulting system is shown to have global and robust stability properties. CCS MPC uses a modulation scheme (SVM/PWM) and yields a closed-loop system that is asymptotically stable. FCS MPC applies the switching states directly and results in a asymptotically set stable closed- loop system.

The associated CFTOC problem is formulated in the normalized $\alpha\beta$ stator flux space that yields a simple dynamic model (integrator), time invariant constraints (voltage vectors, hexagon), but requires a time-varying (rotating) control reference. The control scheme proposes the elimination of the flux–current mapping from the MPC formulation. The current–flux mapping is implemented in the controller as a nonlinear gain. An arbitrarily complex description of this mapping can be used and implemented as a LUT to take saturation and cross-saturation into account. Using an affine approximation, the model accuracy deteriorates to the one obtained with the conventional PMSM model.

References

[1] J. Rodriguez *et al.*, "State of the art of finite control set model predictive control in power electronics," *IEEE Trans. Ind. Informat.*, vol. 9, no. 2, pp. 1003–1016, May 2013.

[2] M. Preindl, E. Schaltz, and P. Thøgersen, "Switching frequency reduction using model predictive direct current control for high power voltage source inverters," *IEEE Trans. Ind. Electron.*, vol. 58, no. 7, pp. 2826–2835, Jul. 2011.

[3] M. Preindl and S. Bolognani, "Model predictive direct torque control with finite control set for PMSM drive systems, Part 1: Maximum torque per ampere operation," *IEEE Trans. Ind. Informat.*, vol. 9, no. 4, pp. 1912–1921, Nov. 2013.

[4] M. Preindl and S. Bolognani, "Model predictive direct torque control with finite control set for PMSM drive systems, Part 2: Field weakening operation," *IEEE Trans. Ind. Informat.*, vol. 9, no. 2, pp. 648–657, May 2013.

[5] E. J. Fuentes, C. Silva, and J. I. Yuz, "Predictive speed control of a two-mass system driven by a permanent magnet synchronous motor," *IEEE Trans. Ind. Electron.*, vol. 59, no. 7, pp. 2840–2848, Jul. 2012.

[6] M. Preindl and S. Bolognani, "Model predictive direct speed control with finite control set of PMSM drive systems," *IEEE Trans. Power Electron.*, vol. 28, no. 2, pp. 1007–1015, Feb. 2013.

[7] M. Preindl and E. Schaltz, "Sensorless model predictive direct current control using novel second-order PLL observer for PMSM drive systems," *IEEE Trans. Ind. Electron.*, vol. 58, no. 9, pp. 4087–4095, Sep. 2011.

[8] S. A. Davari, D. A. Khaburi, F. Wang, and R. M. Kennel, "Using full order and reduced order observers for robust sensorless predictive torque control of induction motors," *IEEE Trans. Power Electron.*, vol. 27, no. 7, pp. 3424–3433, Jul. 2012.

[9] S. Bolognani, S. Bolognani, L. Peretti, and M. Zigliotto, "Design and implementation of model predictive control for electrical motor drives," *IEEE Trans. Ind. Electron.*, vol. 56, no. 6, pp. 1925–1936, Jun. 2009.

[10] S. Mariethoz and M. Morari, "Explicit model-predictive control of a PWM inverter with an LCL filter," *IEEE Trans. Ind. Electron.*, vol. 56, no. 2, pp. 389–399, Feb. 2009.

[11] P. Cortés, M. P. Kazmierkowski, R. M. Kennel, D. E. Quevedo, and J. Rodríguez, "Predictive control in power electronics and drives," *IEEE Trans. Ind. Electron.*, vol. 55, no. 12, pp. 4312–4324, Dec. 2008.

[12] M. Naouar, A. Naassani, E. Monmasson, and I. Slama-Belkhodja, "FPGA-based predictive current controller for synchronous machine speed drive," *IEEE Trans. Power Electron.*, vol. 23, no. 4, pp. 2115–2126, Jul. 2008.

[13] M. Curkovic, K. Jezernik, and R. Horvat, "FPGA-based predictive sliding mode controller of a three-phase inverter," *IEEE Trans. Ind. Electron.*, vol. 60, no. 2, pp. 637–644, Feb. 2013.

[14] M. Preindl and S. Bolognani, "Optimal state reference computation with constrained MTPA criterion for PM motor drives," *IEEE Trans. Power Electron.*, vol. 30, no. 8, pp. 4524–4535, Aug. 2015.

[15] T. Geyer, "Model predictive direct torque control: Derivation and analysis of the state-feedback control law," *IEEE Trans. Ind. Appl.*, vol. 49, no. 5, pp. 2146–2157, Sep./Oct. 2013.

[16] D. Q. Mayne, J. B. Rawlings, C. V. Rao, and P. O. M. Scokaert, "Constrained model predictive control: Stability and optimality," *Automatica*, vol. 36, pp. 789–814, 2000.

[17] F. Borrelli, A. Bemporad, and M. Morari, *Predictive Control for Linear and Hybrid Systems*. Cambridge, U.K.: Cambridge Univ. Press, 2011.

[18] R. P. Aguilera and D. E. Quevedo, "On the stability of MPC with a finite input alphabet," in *Proc. 18th IFAC World Congr.*, 2011, pp. 7975–7980.

[19] R. P. Aguilera and D. E. Quevedo, "On stability and performance of finite control set MPC for power converters," in *Proc. Workshop Predictive Control Elect. Drives Power Electron. (PRECEDE)*, 2011, pp. 55–62.

[20] Y. Wang and S. Boyd, "Fast model predictive control using online optimization," *IEEE Trans. Control Syst. Technol.*, vol. 18, no. 2, pp. 267–278, Mar. 2010.

[21] S. Richter, S. Mariéthoz, and M. Morari, "High-speed online MPC based on a fast gradient method applied to power converter control," in *Proc. Amer. Control Conf. (ACC)*, 2010, pp. 4737–4743.

[22] M. Preindl, C. Danielson, and S. Bolognani, "Model predictive torque control with PWM using fast gradient method," in *Proc. 28th Annu. IEEE Appl. Power Electron. Conf. Expo. (APEC)*, 2013, pp. 2590–2597.

[23] L. Montejano, "Some results about Minkowski addition and difference," *Mathematika*, vol. 43, pp. 265–273, 1996.

[24] E. Kerrigan and J. Maciejowski, "Invariant sets for constrained nonlinear discrete-time systems with application to feasibility in model predictive control," in *Proc. IEEE 39th Conf. Decis. Control (CDC)*, 2000, pp. 4951–4956.

[25] M. Preindl, "Novel model predictive control of a PM synchronous motor drive," Ph.D. dissertation, Dept. Ind. Eng., Univ. Padua, Padua, Italy, 2014.

[26] Z. Artstein, "Stabilization with relaxed controls," *Nonlinear Anal.: Theory Methods Appl.*, vol. 7, pp. 1163–1173, 1983.

[27] D. Muñoz de la Peña and P. D. Christofides, "Lyapunov-based model predictive control of nonlinear systems subject to data losses," *IEEE Trans. Autom. Control*, vol. 53, no. 9, pp. 2076–2089, Oct. 2008.

[28] P. D. Christofides, J. Liu, and D. Muñoz de la Peña, *Lyapunov-Based Model Predictive Control*. New York, NY, USA: Springer, 2011.

[29] D. Luenberger and Y. Ye, *Linear and Nonlinear Programming*. New York, NY, USA: Springer, 2008.

[30] T. Geyer, "Computationally efficient model predictive direct torque control," *IEEE Trans. Power Electron.*, vol. 26, no. 10, pp. 2804–2816, Oct. 2011.

[31] T. Geyer and D. Quevedo, "Multistep finite control set model predictive control for power electronics," *IEEE Trans. Power Electron.*, vol. 29, no. 12, pp. 6836–6846, Dec. 2014.

Matthias Preindl (S'12–M'15) received the B.Sc. degree in electrical engineering (*summa cum laude*) from the University of Padua, Padua, Italy, the M.Sc. degree in electrical engineering and information technology from ETH Zurich, Zurich, Switzerland, and the Ph.D. degree in energy engineering from the University of Padua, in 2008, 2010, and 2014, respectively.

He was an R&D Engineer of Power Electronics and Drives, Leitwind AG, Sterzing, Italy (2010–2012), a Post Doctoral Research Associate with the McMaster Institute for Automotive Research and Technology, McMaster University, Hamilton, ON, Canada (2014–2015), and a Sessional Professor in the Department of Electrical and Computer Engineering, McMaster University, Hamilton, ON, Canada (2015). He is currently an Assistant Professor in the Department of Electrical Engineering, Columbia University in the City of New York, NY, USA. His research interests include the design and control of power electronic and motor drive systems with applications in electrified transportation systems, renewable-energy power plants, and smart grids.